Two-component fullerene molecular layers assembled on the Au(111) substrate

Guo, Quanmin

DOI:
10.1021/acs.jpcc.8b06420
https://pubs.acs.org/doi/10.1021/acs.jpcc.8b06420

Two-component Fullerene Molecular Layers Assembled on the Au(111) Substrate

Yitao Wang[1], Lu'an Guo[1,2], Quanmin Guo*[*1]

1. School of Physics and Astronomy, University of Birmingham, Birmingham B15 2TT, United Kingdom.

2. Department of Applied Physics and Key Laboratory for Quantum Information and Quantum Optoelectronic Devices of Shaanxi Province, Xi'an Jiao-Tong University, Xi'an, Shaanxi, 710049, PR China.

Abstract

Self-assembly of binary and multi-component colloidal crystals is an effective approach for the fabrication of structured new materials. The formation of colloidal crystals in most cases is controlled by optimized space occupation by the particles. C_{60} and C_{70} molecules, when treated as the smallest "colloidal particles", can be used as model systems to study the formation of multicomponent molecular crystals in which the intermolecular forces are mainly of the van der Waals type. By deposition of C_{60} and C_{70} molecules onto Au(111), the mixing of the two molecules has been investigated. Both C_{60} and C_{70} form close-packed layers on Au(111), but with different lattice constants. At room temperature, the molecules within the molecular layer have complete freedom to rotate. The boundary between the C_{60} and the C_{70} domains consists of row dislocations. Adding C_{60} onto a C_{70} layer has an interesting effect in that C_{60} molecules can push their way into the C_{70} layer and force the C_{70} molecules to take a fixed upright configuration where the long axis of the molecule is perpendicular to the interface. Significant interlayer diffusion takes place at elevated temperatures. When C_{70} is added to a C_{60} layer, there is little evidence of C_{70} getting into the C_{60} layer. The second layer C_{70} forms a lattice-matched structure by taking the upright orientation.

Keywords: Self-assembly; Molecular monolayers; Fullerene; Scanning tunneling microscopy; epitaxy; lattice-mismatch; interface; van der Waals solids.

* Email: Q.Guo@bham.ac.uk

1. Introduction

Multicomponent materials with two or more constituent building blocks have great potential technological applications[1-4]. In contrast to single-component materials, multicomponent materials such as metallic glasses[5] and metal organic frameworks[6-7] have a clear advantage that their properties can be fine-tuned by varying the composition, structure and synthesis procedure. One interesting class of multicomponent materials are soft solids formed by close-packing of the constituent particles; for instance, photonic crystals assembled with colloidal particles[8] and binary nanoparticle superlattices (BNSL)[9]. The structure of the solid depends on the size and shape of the building blocks[10]. Being the simplest multicomponent materials, the binary system has attracted a high level of attention. By drying a suspension containing two kinds of particles with polymethylmethacrylate (PMMA) as cores and different radii, Bartlett *et al* [11-12] have studied the binary mixtures of hard sphere colloids and found complex ordered structures such as AB_2 and AB_{13}. The stoichiometry and stability of the BNSL depend on a number of factors including the electrical charge on the colloidal particle and the van der Waals forces [13]. By changing the stoichiometry, two A_3B structures with packing densities higher than that of the phase-separated face-centered cubic crystals have been found with simulation[14]. Kiely *et al* have studied the assembly of superlattices from alkanethiol-passivated gold nanoparticles of different radii[15]. With a radius ratio of the two particles at 0.47, the small and large particles form phase-separated domains. A relatively stable AB_2 phase is formed with a radius ratio in the range from 0.48 to 0.62. A random alloy of gold particles can appear if the size difference is less than 15% as explained by the Hume-Rothery rule[10].

Recently, there has been growing interest in the precise control of the binary superlattices[9,15] as well as the assembly of more complex structures using more than two building blocks[16-18]. A layer-by-layer assembly method was introduced by Denkov *et al* and modified by Singh *et al* for creating binary and ternary colloidal crystals[19,20]. With the method developed by Denkov *et al*, it is possible to grow colloidal crystals by depositing alternating A and B layers with a high degree of accuracy[21-23]. The complexity increases if two particles with not just different sizes, but also different shapes are mixed. In the case of nano-rods and nano-spheres, it is found that phase separation is favoured[24,25]. In a study of a mixture of Fe_3O_4 nanospheres and $NaYF_4$ nano-rods, Ye *et al*[26] observed a bulk separating phase, a lamellar phase and an AB_2 binary nanocrystal shape alloy (BNSA). The BNSAs are stabilized mainly with the help of short-range attractions[26].

The size of the building blocks in binary and tertiary colloidal crystals ranges from several nanometers (gold nanoparticles) to a few micrometers (silica or polymer spheres). The assembly of very small particles with sizes of the order of one nanometer is rarely studied. This is because there are great technological challenges in producing size-selected particles at this scale and that conventional assembly methods

based on a colloidal suspension are hard to operate for such small particles. Buckminster fullerenes such as C_{60} and C_{70} are probably the smallest "colloidal particles". The interaction between these molecules is mainly of the van der Waals type and hence the corresponding molecular crystals consist of layers of closed-packed molecules,[27,28] similar to the hard-sphere packing mode in colloidal crystals of larger spheres. Therefore, C_{60} and C_{70} are good candidates for the study of binary mixtures involving particles of ~ 1nm in size.

Here we investigate the mixing of C_{60} and C_{70} molecules using scanning tunnelling microscopy (STM). We deposit the two molecules sequentially onto a (111)-oriented gold substrate and follow the mixing as we increase the sample temperature. Although C_{60} can be treated approximately as a "spherical" object, C_{70} has a "rugby" shape with an aspect ratio of ~0.89[29-31]. The dimension along the short axis of C_{70} is almost equal to the diameter of C_{60}. The adsorption of fullerene molecules, in particular C_{60}, on Au(111) is a well-studied system[32-42]. There is a strong tendency for the molecules to assemble into close-packed layers on Au(111). The close-packed layer can exist in several phases depending on its azimuthal orientation[33,34,39].

2. Experimental

Experiments were performed using an Omicron Variable-Temperature Scanning Tunnelling Microscope (VT-STM) in an ultra-high vacuum chamber with a base pressure of 5×10^{-10} mbar. The gold sample is a polycrystalline thin film deposited on a highly-oriented pyrolitic graphite (HOPG) substrate. The crystals inside the Au film have their (111) plane parallel to the surface of the HOPG substrate. After the sample is transferred into the UHV system, it is treated by many cycles of Ar+ ion sputtering and thermal annealing. C_{60} and C_{70} molecules (purchased from MER, 99.5% purity) were sublimed onto the HOPG substrate using home-built effusion cells. During sublimation, the C_{60} cell and the C_{70} cell were kept at 554 K and 601 K, respectively. Under these temperatures, the deposition rate is around 0.1 monolayer(ML) per minute. Before sublimation, the cells were degased at 500 K for 5 minutes. Deposition is mostly conducted when the sample is kept at room temperature (RT). Imaging is performed soon after deposition to determine the degree of molecular mixing at RT. The sample is annealed step by step to higher temperatures. After annealing at each temperature for one hour, STM images are acquired once the sample is cooled to RT.

3. Results and Discussion

3.1 The first molecular layer

Both C_{60} and C_{70} form close-packed molecular layers on Au(111). The Au(111) substrate is rather flexible and has a tendency to appear in various reconstructed forms [43,44]. The exact form of reconstruction depends on the extent of charge transfer at the interface. For this reason, a single layer of C_{60} on Au(111) contains molecules in nonequivalent bonding configurations[33,34,39]. In contrast, fullerene layers formed on

HOPG have a much simpler structure because the HOPG substrate has no freedom to reconstruct and it serves as a simple, "inert", platform. Here we briefly discuss the features of C_{60} and C_{70} layers formed on HOPG and use the C_{60}/C_{70}-HOPG system as a useful reference.

3.1.1 C_{60} and C_{70} on HOPG

Figure 1 shows an STM image acquired from a HOPG sample which is covered by a single layer of molecules. The C_{60} and C_{70} molecules are deposited sequentially at RT. The sample is then thermally annealed to 470 K which leads to some intermixing of the molecules. In this image, one can see separate domains of C_{60} and C_{70}. The C_{60} domain and the C_{70} domain have different lattice parameters. The nearest neighbor C_{60}-C_{60} distance within the C_{60} domain is 1.0 nm; the nearest neighbor C_{70}-C_{70} distance within the C_{70} domain is 1.07 nm. The C_{70} molecules within the C_{70} domain are 0.08 nm taller than C_{60} molecules within the C_{60} domain as measured by the STM. Inside the C_{60} domain, the scattered C_{70} molecules are 0.11 nm taller than the surrounding C_{60} molecules. Although height measured by STM has electronic contributions as well as geometric contributions, the features in Fig. 1 indicate that the height differences are mainly of geometric in nature. Therefore, the C_{70} molecules trapped inside the C_{60} domain have their long axis perpendicular to the substrate. The 0.11 nm height difference is consistent with the geometric height difference between a C_{60} and upright C_{70}. By having the long axis perpendicular to the substrate, a trapped C_{70} molecule inside the C_{60} domain has the same footprint as a C_{60}. This is a favorable configuration because it leads to almost zero strain into the C_{60} lattice by substituting a C_{60} with a C_{70}. The C_{70} molecules inside the C_{70} domain do not have a fixed orientation at room temperature and they are able to rotate about both the long and short axes. The height for such free-rotating molecules can be regarded as an effective height which is derived from a C_{70} molecule switching between lying down and upright configurations. The crystalline form of C_{70} has an fcc structure at temperatures above 340 K. In this fcc phase, the C_{70} molecule rotates freely with no orientational order. The nearest neighbor distance in the fcc phase is 1.06 nm[45]. Below 340 K, a phase transition occurs such that the long axis of the C_{70} molecule becomes frozen in the direction perpendicular to one of the close-packed layers. As a consequence, the in-plane nearest neighbor C_{70}-C_{70} distance is reduced from 1.06 nm to 1.01 nm. The 1.07 nm nearest neighbor C_{70}-C_{70} distance measured by our STM is a good indication that the C_{70} molecules within the first C_{70} layer on HOPG are rotationally disordered even at RT[46].

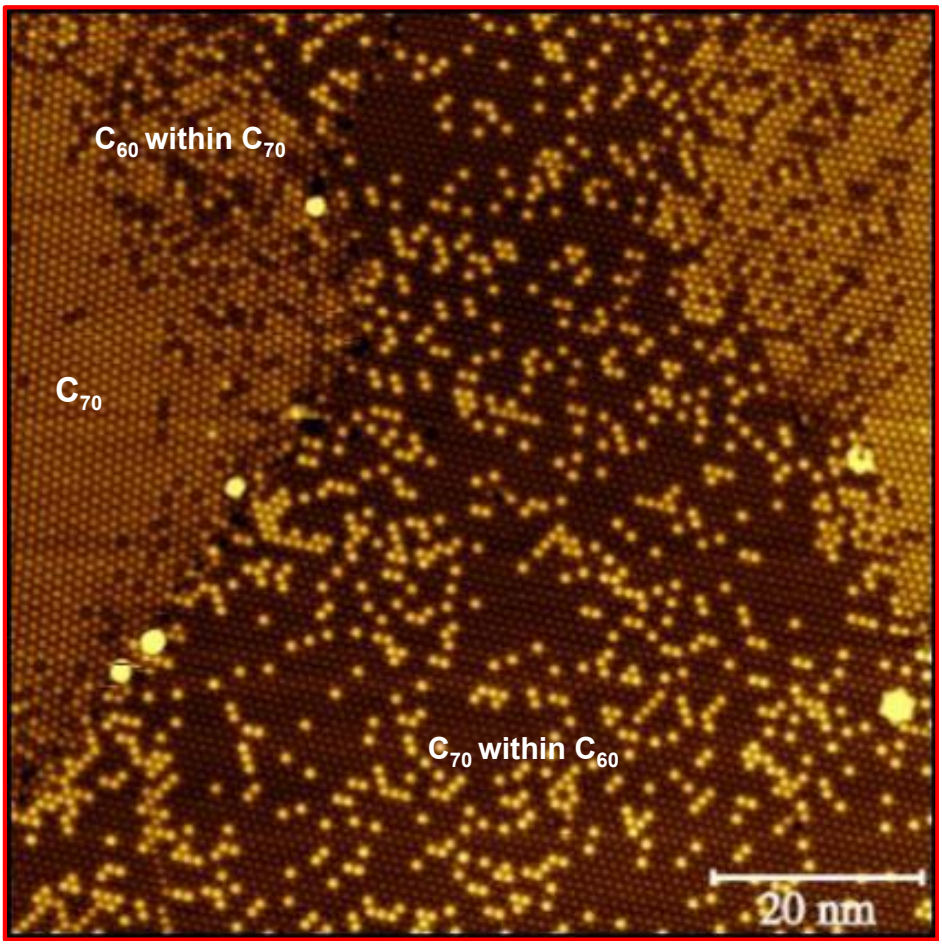

Figure 1. Close-packed single molecular layer consisting of phase-separated of C_{60} and C_{70} on HOPG. The molecules are deposited sequentially onto HOPG at RT. Thermal annealing to 475 K for 30 minutes has caused some mixing. Separate C_{60} and C_{70} domains are formed. Within the C_{60} domain, there are scattered C_{70} molecules that have substituted C_{60} molecules. The image, 90 nm × 90 nm, is collected using –2.1 V sample bias voltage and 100 pA of tunneling current.

3.1.2 C_{60} and *C_{70} on Au(111)*

With the finding for C_{60} and C_{70} on HOPG in the previous section serving as a reference, we can now discuss the behavior of the molecules on Au(111). In comparison with HOPG, the Au(111) substrate is more complicated due to the presence of surface reconstruction. Figure 2(a) is an STM image from Au(111) covered by ~ 0.65 ML of C_{70}. The molecules are deposited onto the Au(111) substrate at RT and the image is collected at RT. Most of the Au(111) is covered by a single layer of C_{70}. The single layer C_{70} is 0.7 nm above the Au(111) substrate as measured directly from the STM image. This is in contrast to the 1.0 nm height measured for C_{70} on HOPG. 1.0 nm more or less reflects the true physical dimension of C_{70}. On Au(111), the electronic contrast between Au(111) and C_{70} causes a much reduced apparent height of the molecule. Since we have no complimentary atomic force microscopic measurement, it is not clear if the 0.3 nm height difference measured from the two different substrates is purely due to different contributions from the density of states. A small fraction of the Au(111) substrate remains uncovered. Near

the top left corner of the image, there are a few patches of second layer C_{70}. The second layer C_{70} is ~0.8 nm taller than the first layer. This is comparable to what is found for the second layer C_{70} on HOPG. The edges of the second layer C_{70} islands are very sharp, suggesting that the edges are stationary at RT. In contrast, the edges of the first layer C_{70} appear hairy, indicating that the edges are under constant change by losing and capturing molecules. The C_{70} molecules are close-packed along the direction of the discommensuration lines of Au(111). Hence this particular C_{70} structure is called the R30^o phase because the close-packing direction of the molecules is rotated by 30 degrees from the close-packing direction of Au atoms. Despite the similarity with the $(2\sqrt{3} \times 2\sqrt{3})$R30° phase of C_{60} on the same surface, the structure of the C_{70} layer shown in Fig. 2(a) cannot be named $(2\sqrt{3} \times 2\sqrt{3})$R30° because the underlying substrate is still in its reconstructed form. Apart from the R30^o phase, other frequently observed phases are R0^o and R14^o, similar to what is reported for C_{60}[34,37]. The close-packed layer usually forms by nucleation along step edges. Thus, if the first row of molecules align themselves along a step edge consisting of close-packed Au atoms, the resulting molecular domain will have molecules close-packed also along the same direction of the Au atoms.

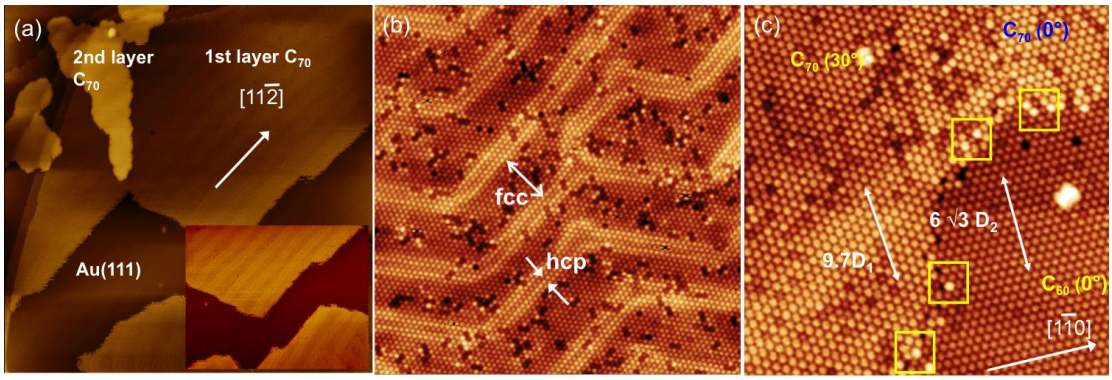

Figure 2. (a) STM image (200 nm × 200 nm, –2.5 V, 80 pA) of Au(111) covered with 0.3 ML of C_{70} at room temperature. One of the close-packing directions of C_{70} molecules is parallel to the discommensuration lines. The herringbone reconstruction of the Au(111) substrate under the 30° C_{70} islands remains unchanged. (b) Morphology of the C_{70} layer after annealing at 573 K for one hour. (75 nm × 75 nm, -2.5V, 100pA). The discommensuration lines have been modified due to the enhanced interaction between C_{70} and gold, leading to a clear broadening of the fcc region and narrowing of the hcp region. After annealing, dark defects have appeared in the fcc regions. (c) STM image (60 nm × 60 nm, -2.5V, 100pA) showing 0.3 ML C_{60} molecules deposited onto Au(111), followed by 0.3 ML C_{70}. R0° C_{60}, R0° and R30° C_{70} are shown in the image. The domain boundary between R0° C_{70} and R0° C_{60} islands is fuzzy while a relatively sharp boundary is formed between the R30° C_{70} and R0° C_{60} islands.

As can be seen in Fig. 2(a), the herringbone reconstruction of the Au(111) surface remains unchanged after a layer of C_{70} is added. This is can be seen more clearly in the inset which is part of the image after applying contrast enhancement. This suggests a rather weak molecule-substrate interaction. This is in contrast to C_{60}, which

upon adsorption, can readily lift the herringbone reconstruction at RT[37]. Lifting the herringbone reconstruction of Au(111) is a rather reliable signature that a significant amount of electron charge transfer from the substrate to the molecule has taken place[47]. The inability of C_{70} to lift the reconstruction indicates that the charge transfer from Au(111) to C_{70} is not as extensive as that for C_{60}. The interaction between C_{70} and Au(111) is strong enough to modify the herringbone reconstruction when the sample is heated to temperatures above 550 K. As can be seen in Fig. 2(b), after heating to 573 K, the familiar feature of the herringbone pattern is still visible. However, the width of the fcc domain, highlighted by a double-headed arrow in Fig. 2(b), has expanded to about 10 nm which is much broader than that on the clean Au(111) surface. The hcp domain remains narrow at about 1 nm. The density of discommensuration lines is reduced by ~ 50%. Adsorbate-induced broadening of the fcc domain of the herringbone reconstruction has also been observed for other molecules[48]. The broadening of the fcc domain is the initial step towards the complete lifting of the herringbone reconstruction. Within the fcc region, we find a small number of "dim" molecules. Below these dim molecules, there are probably atomic defects in the Au(111) surface due to the fact that the fcc region is still under stress.

Fig. 2(c) shows an STM image from an area with adjoining C_{60} and C_{70} domains. The sample is prepared by the deposition of 0.3 ML of C_{60}, which is followed by an extra 0.3 ML of C_{70}. The C_{60} domain in the image belongs to the $R0^o$ phase. For C_{70}, there are two rotational domains. The majority of the C_{70} molecules are found in an $R30^o$ domain. A small fraction of C_{70} molecules, near the top right hand corner of the image, form an $R0^o$ domain. Therefore, we have a C_{70}-$R0^o$/C_{60}-$R0^o$ domain boundary and a C_{70}-$R30^o$/C_{60}-$R0^o$ domain boundary.

A doubled headed arrow is used as a ruler to measure the nearest neighbor distances for both C_{60} and C_{70}. In the C_{70}-$R30^o$ domain, the length of the doubled headed arrow equals to 9.7 D_1 where D_1 is the nearest C_{70}-C_{70} distance. The same distance equals to $6\sqrt{3}$ D_2 where D_2 is the nearest C_{60}-C_{60} distance within the C_{60}-$R0^o$ domain. Since the measurement is performed in the same direction, we can obtain a rather accurate D_1/D_2 ratio without worrying about scanner calibration or thermal drift. From this measurement, we find the ratio of the lattice parameters between C_{70} and C_{60} is 1.07. This ratio is identical to what we measured on the HOPG substrate. Therefore, we can safely conclude that the molecules within the first layer C_{70} on Au(111) are in their free-rotating state. There are a small number of tall molecules marked with the yellow squares near the domain boundaries. These molecules are taller than those within the close packed C_{70} domain and are thus identified as C_{70} molecules having their long axis fixed in the direction perpendicular to the substrate surface.

The C_{70}-$R30^o$/C_{60}-$R0^o$ domain boundary in Fig. 2(c) is typical of the boundaries occurring between two rotationally misaligned domains of close packed hard spheres. The coordination number for molecules at such domain boundaries is reduced from 6 to 5, or lower, corresponding to a reduced surface coverage at the boundary. The

$R30^o/R0^o$ domain boundary can be found between a C_{70} and a C_{60} domain, or between two C_{70} (or two C_{60}) domains. Figure 3(a) shows such a boundary between two C_{70} domains. The $R0^o/R0^o$ or $R30^o/R30^o$ domain boundary, on the other hand, forms only between a C_{70} domain and a C_{60} domain. This type of boundary is formed as a result of lattice mismatch. A C_{70}-$R30^o/C_{60}$-$R30^o$ boundary can be found in Fig. 3(b) (Inset) where a row of C_{60} terminates at the boundary, giving rise to an edge dislocation. Fig. 3(c) shows a very straight and sharp C_{70}-$R30^o/C_{60}$-$R30^o$ boundary. A magnified view of this boundary is shown in Fig. 3(d) where we find that a distance covered by 20 rows of C_{70} can accommodate 21 rows of C_{60}. Thus, the nearest neighbour distance for C_{70} is 1.05 times of that for C_{60}. This is smaller than what was found from Fig. 2(c). Assuming a constant nearest neighbor distance for C_{70}, our finding suggests that the C_{60} molecules have a larger nearest neighbour distance in the $R30^o$ phase than that in the $R0^o$ phase. It is expected that the nearest neighbour distance between fullerene molecules depends on the strength of the molecule-substrate interaction. Fig. 3(e) shows a small section of a C_{70}-$R30^o/C_{60}$-$R30^o$ boundary. Dashed lines are drawn into the image to show the positional relationship between the C_{60} rows on one side of the boundary and the C_{70} rows on the other side. As one moves from the first dashed line, 1, to the sixth dashed line, 6, the molecular rows on the two sides become gradually offset due to the different row-row distances.

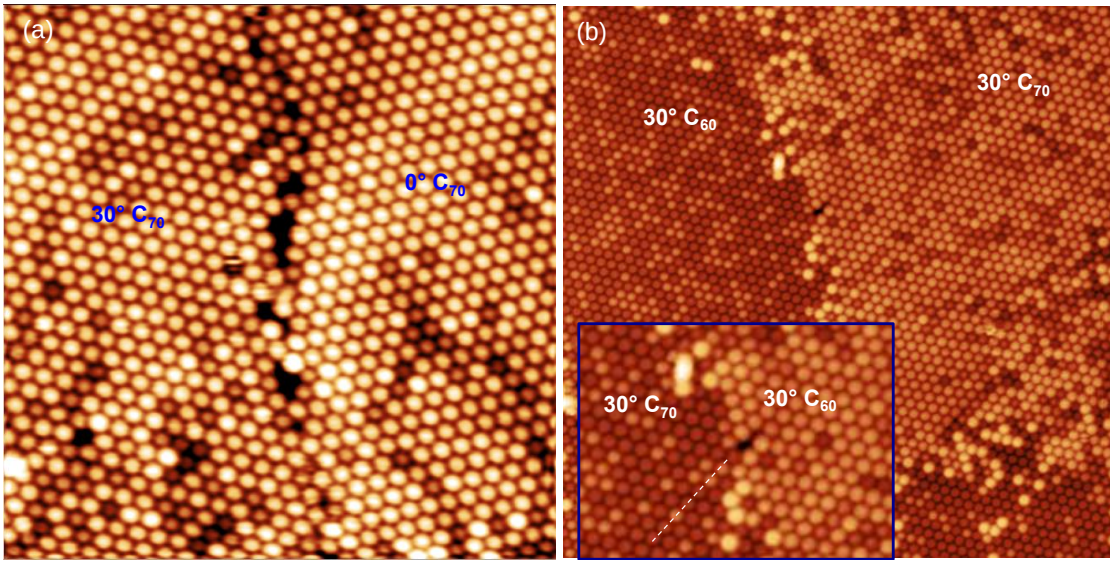

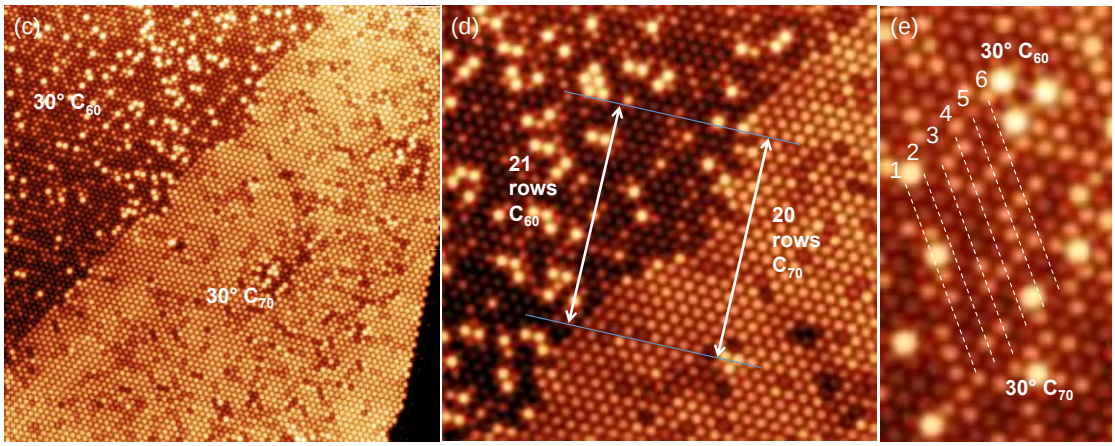

Figure 3. (a) STM image (30 nm × 30 nm, –2.5 V, 100 pA) showing the boundary between R0° and R30° C_{70} domains. The boundary separating these two domains is similar to the R0° C_{60} and R30° C_{60} boundary. (b) An R30° C_{60} and R30° C_{70} domain boundary. (55 nm × 55 nm, –2.5 V, 100 pA). Inset shows how an row of C_{60} terminates at the boundary. (c) A sharp and straight R30° C_{60} and R30° C_{70} domain boundary. (85 nm × 85 nm, –2.5 V, 100 pA). (d) Larger nearest neighbor distance for C_{70}. (e) Mismatching rows at the domain boundary indicating weak coupling between C_{60} and C_{70} across the boundary.

Figure 4(a) shows an STM image obtained after annealing the sample to 573 K which is high enough to thermally desorb all molecules from the second layer. During annealing at 573 K, the thermal energy is likely to be sufficient to drive the first layer into a liquid-like phase. The C_{60}-rich and C_{70}-rich domains observed in Fig. 4(a) are probably formed during the cooling down period from 573 K to RT. It is clear that C_{60} and C_{70} do not form a homogeneous layer. Instead, they phase separate into C_{60}-rich and C_{70}-rich domains. The image in Fig. 4(b) shows scattered C_{70} molecules trapped inside an R30° C_{60} domain. For the R0° C_{60} domain near the lower left corner of Fig. 4(a), trapped C_{70} molecules are mainly found in the vicinity of the boundaries. In Fig. 4(c), we see C_{70} molecules mixed into the R0° C_{60} domain. It is not yet clear to us why part of the R0° C_{60} domain in Fig. 4(c) remains free of C_{70} molecules. Fig. 4(d) shows an R30° C_{70} domain with two patches of close-packed C_{60} molecules. It seems that C_{60} molecules inside the C_{70}-rich domain prefer to aggregate into C_{60} islands rather than staying as scattered individual molecules. In Fig. 4(b), the tallest molecules are identified as C_{70} molecules. The C_{60} molecules in Fig. 4(b) appear with different heights due to the different ways that a C_{60} can interact with the Au(111) substrate. Height profiles along the lines A-B, C-D, and E-F are presented in Fig. 4(e), (f) and (g), respectively. An easy way to separate C_{70} molecules from C_{60} molecules of various apparent heights is to conduct imaging at different bias voltages. Fig. 5 shows STM images acquired at four different sample bias voltages. The images collected using +2.5 V and -2.5 V are affected by the molecular orbitals of the fullerene molecules. For bias voltages of smaller magnitude, tunnelling via molecular orbitals diminishes, so the measured height contrast reflects more or less the

geometric height of the molecules. The images in Fig. 5 (b) and (d) give a clear contrast between C_{60} and C_{70} molecules.

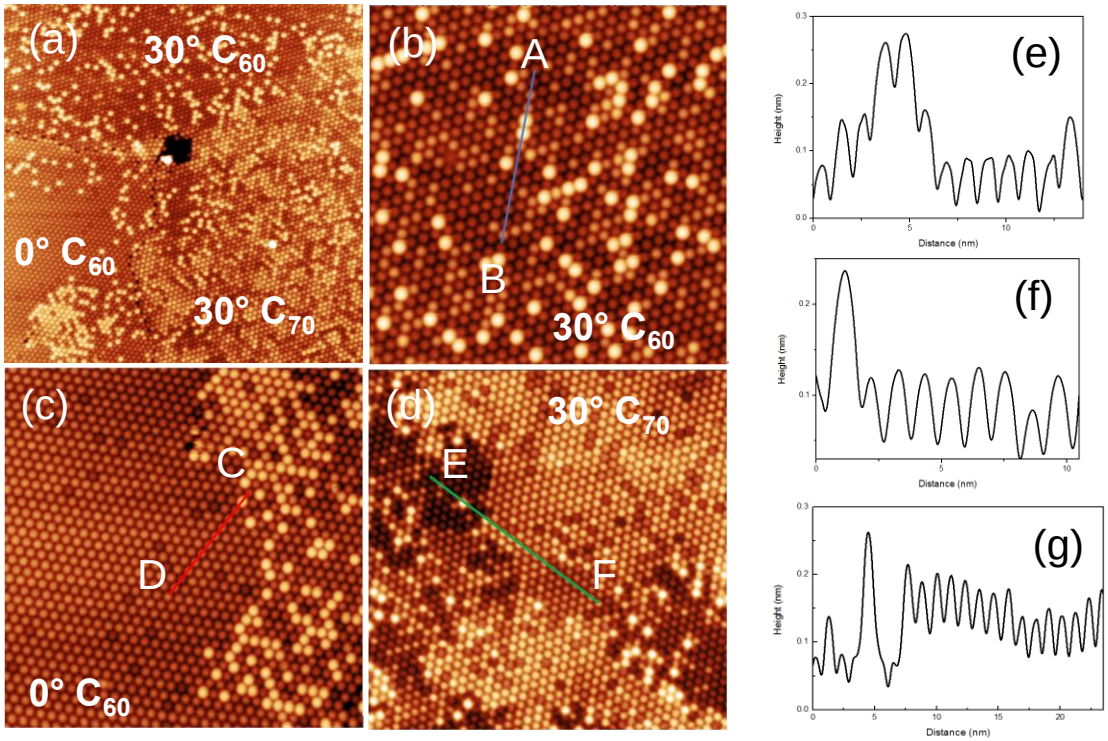

Figure 4. (a) STM image (75 nm × 75 nm, –2.5 V, 100 pA) showing the mixture of C_{60}-R30°, C_{60}-R0° and C_{70}-R30° domains on Au (111). (b) In the R30° C_{60}–rich domain, C_{60} molecules appear with different apparent heights due to their varied bonding to the Au(111) substrate. Standing out from the C_{60} molecules, the trapped C_{70} molecules are clearly identified as features 0.10 nm higher than the highest C_{60} molecules. Height profile along line A-B is displayed in (e). (30 nm × 30 nm, -2.5 V, 100 pA) (c) C_{70} molecules mixing into the R0° C_{60} domain. (35 nm × 35 nm, -2.5 V, 100 pA) (d) C_{60} islands formed within a C_{70}-rich domain. (40 nm × 40 nm, -2.5 V, 100 pA) (e) Line profile showing that trapped C_{70} (b) are 0.1 nm taller than C_{60}. These trapped C_{70} molecules have an upright orientation. The height difference between bright and dark C_{60} in the background is around 0.05 nm. (f) Line profile along line C-D in (c) showing the height difference between C_{70} and C_{60}. (g) Line profile along line E-F in (d).

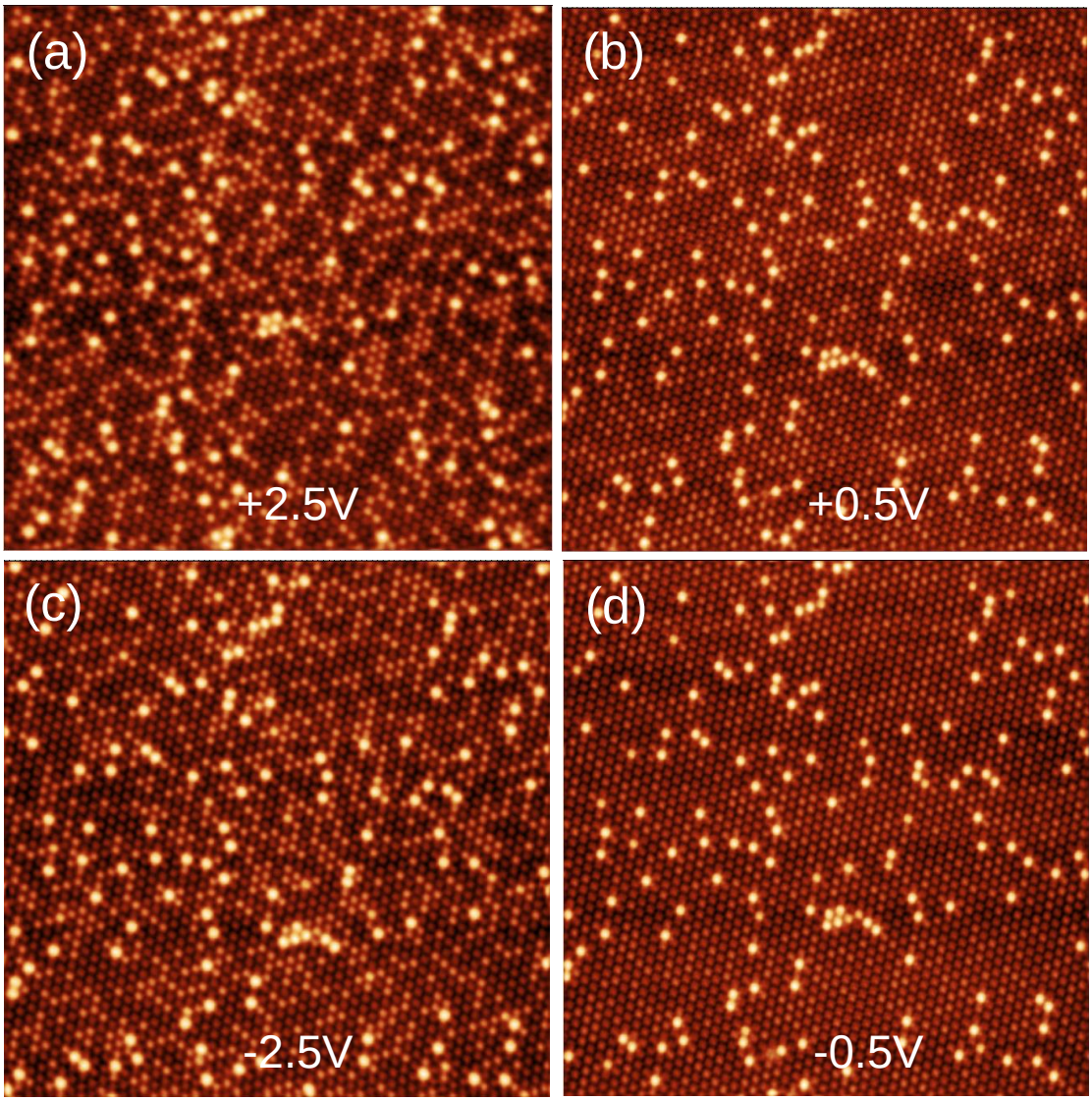

Figure 5. STM images (30 nm × 30nm) from the same area with the same tunnelling current of 100 pA but different sample bias voltages. (a) 2.5 V. (b) 0.5 V. (c) –2.5 V. (d) –0.5 V. For the bias voltages of ± 0.5 V, contribution from molecular orbitals is minimised allowing the clear separation of the molecules according to their different physical heights.

3.2 Interlayer diffusion

In the following sections, we examine the interaction between two layers of molecules: a layer of C_{60} and a layer of C_{70}. We investigate how molecules move from one layer to another. The sample is prepared by depositing more than one layer of C_{60} or C_{70} to make sure that no part of the Au(111) substrate is exposed. The sample is then heated to 500 K to desorb the molecules from the second and third layers. This leaves the sample almost fully covered by a single layer of C_{60} or C_{70}. On top of this single layer C_{60} or C_{70}, we then add 0.65 ML of C_{70} or C_{60} at RT. Depending on the deposition sequence, we have either a C_{60}-on-C_{70} or C_{70}-on-C_{60} system. We follow changes to these systems as the sample is gradually heated to high temperatures. We pay particular attention to the transport of molecules between the two contacting layers.

3.2.1 0.65ML C_{60} deposited on top of 1.0 ML C_{70} (C_{60}-on-C_{70})

Deposition of C_{60} onto a C_{70} monolayer at RT leads to two interesting observations: i) incorporation of C_{60} into the C_{70} monolayer; and ii) formation of dark bands in the newly grown C_{60} layer above the C_{70}. The STM image in Figure 6(a) shows the formation of second layer C_{60} on top of a C_{70} monolayer. Fig. 6(b) is an STM image from an area covered by the first monolayer of C_{70} only. The incorporation of C_{60} into the C_{70} layer is clearly identified by the presence of dark rows of molecules. The dark rows are ~ 0.1 nm deep and consists of C_{60} molecules. Thus, during deposition, C_{60} molecules landing onto the C_{70} layer are able to squeeze into the C_{70} layer. This would increase the total molecular density and hence force the C_{70} molecules to switch from a state of random rotation to one that has the long molecular axis perpendicular to the substrate. The STM image in Fig. 6(c) shows the morphology of the newly formed C_{60} layer. The C_{60} layer consists of close-packed C_{60} molecules. What is interesting is the appearance of dark bands within the C_{60} layer. The dark bands, ~1-2 molecules wide, connect to one another forming a network. A height profile, Fig. 6(d), shows that the dark bands are ~0.1nm deep. When C_{60} molecules are deposited onto a C_{60} monolayer, there are no such kinds of dark bands[48]. Moreover, there are no dark bands in the original C_{70} monolayer. Therefore, the formation of the bands is a direct consequence of the interaction between the top C_{60} layer and the bottom C_{70} layer. As shown already in Fig. 6(b) that C_{60} molecules can drop down into the C_{70} layer and form rows of C_{60}, the dark bands in Fig. 6(c) are very likely caused by the same process. Inserting C_{60} molecules into the C_{70} layer forces the C_{70} molecules to take an upright orientation and a reduced nearest neighbor distance. When C_{70} molecules are all oriented with their long axis perpendicular to the substrate, the C_{70}-C_{70} distance within the C_{70} layer matches the C_{60}-C_{60} distance within the C_{60} layer. This would lead to a nearly strain free interface between the C_{60} and C_{70} layers. Within the dark bands in Fig. 6(c), the second layer C_{60} molecules are sitting above C_{60} molecules. Due to the intrinsic lattice mismatch between C_{60} and C_{70}, when a layer of C_{60} is placed upon a layer of C_{70}, the strain at the interface tends to exert a compressive stress on the C_{70} layer and an tensile stress on the C_{60} layer. The ability of the C_{70} molecule to move from a random rotating state to a fixed upright configuration minimizes the interfacial strain[46].

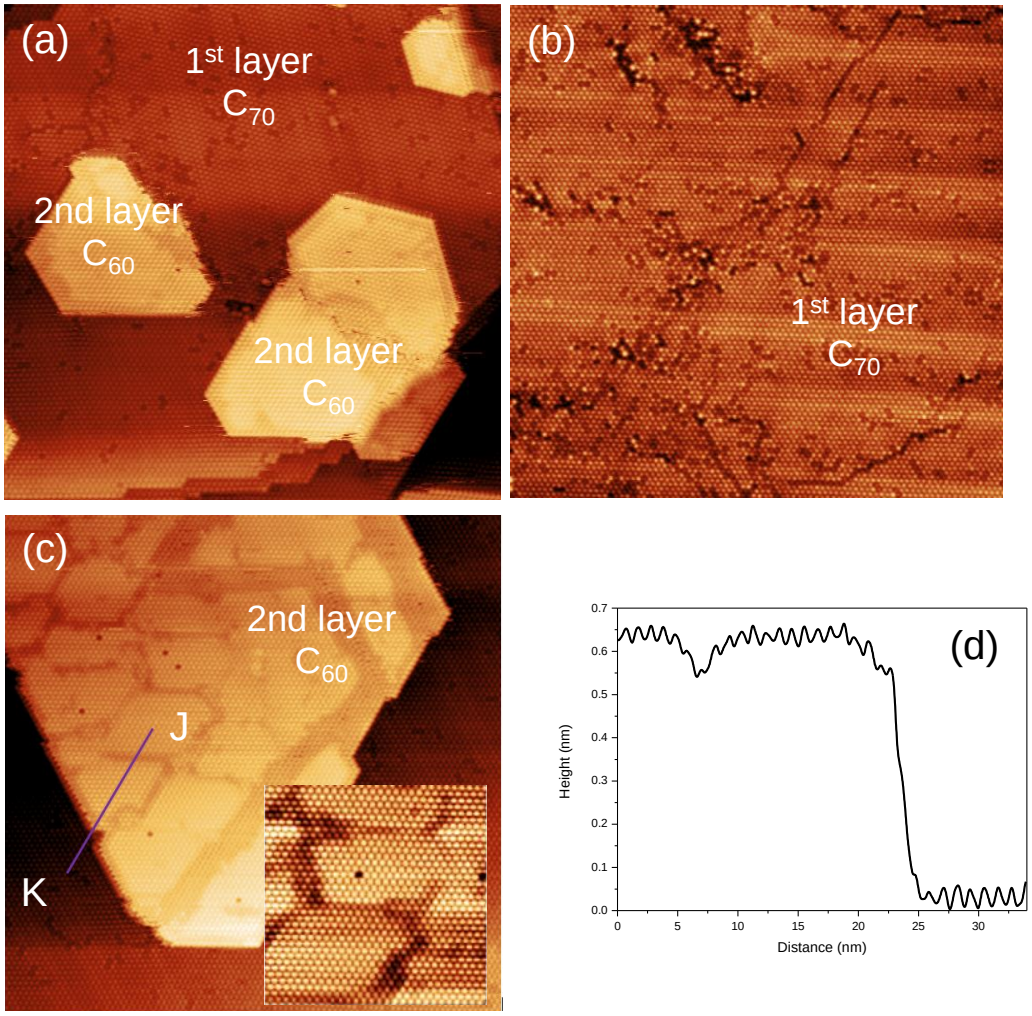

Figure 6. (a) STM image, (95 nm × 95 nm, -2.5V, 100 pA), showing C_{60} islands formed on top of one compact monolayer of C_{70}. (b) Upon landing on the C_{70} monolayer, a small number of C_{60} molecules manage to get into the C_{70} layer and form "dark" rows of C_{60}. (85 nm × 85 nm, -2.5 V, 100 pA). (c) STM image (100 nm × 100 nm, -2.5 V, 100 pA) showing a second layer C_{60} island sitting on the C_{70} monolayer. A network of dark bands is observed. Inset (40 nm × 50 nm, -2.5 V, 100 pA) shows that molecules inside the dark bands are orderly spaced and there is no obvious defects around the bands. (d) Line profile showing the height change along line J-K in (c). The dark bands are 0.08 nm to 0.10 nm deep. The height of the C_{60} island is 0.65 nm taller than the background C_{70}.

The network of dark bands persists as the sample is heated to higher temperatures. Figure 7(a) shows an image acquired after annealing the sample to 423 K for one hour. Within the second layer C_{60} islands, a small number of bright spots have appeared. These bright spots are mainly isolated individual spots, although there are also a small number of dimers. They prefer not to form in the dark bands or the edges of islands. Judging from their apparent heights, these bright spots are identified as C_{70} molecules. Since there were no C_{70} molecules in the second layer of the initial sample, these C_{70} molecules can only come from the C_{70} layer below. This suggests that, during annealing at 423 K, further exchange between C_{60} and C_{70} has taken place across the

interface. With C_{70} molecules moving up, some C_{60} molecules are expected to drop down to avoid over-crowding of molecules in either layer. As the temperature of the sample is increased to 473 K, more bright spots appear in the C_{60} layer, Fig. 7(b). After annealing to 523 K for one hour, the number of the second layer islands has decreased drastically due to thermal desorption. For the remaining second layer islands, we now see a rather extensive mixing of C_{60} and C_{70} as seen in Fig. 7(c). A height profile along line J-K in (a) is displayed in Fig. 7(d). One can see that C_{70} molecules embedded in the second layer C_{60} is about 0.1 nm taller than C_{60}. C_{60} molecules within the dark bands appear ~ 0.1 nm lower than C_{60} molecules in the same layer.

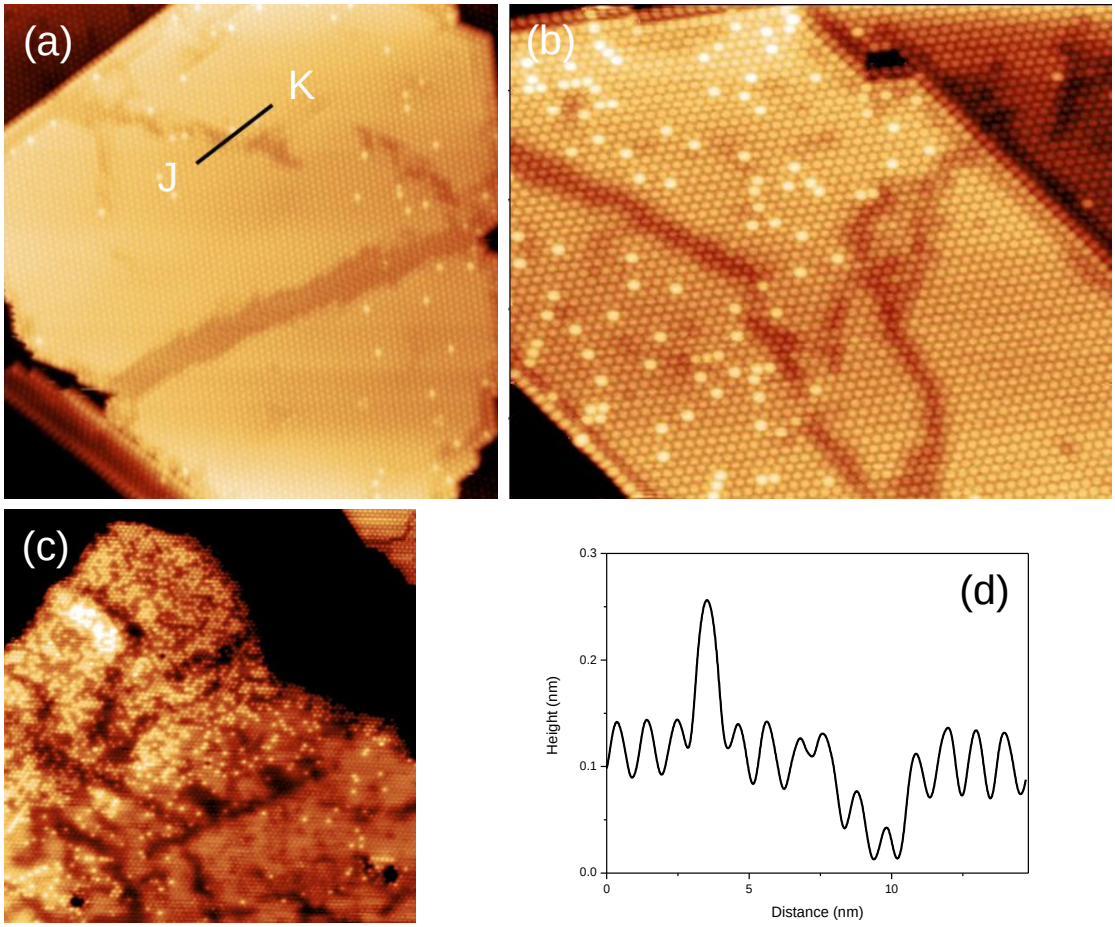

Figure 7. (a) STM image (75 nm × 75 nm, –2.5 V, 100 pA) showing C_{60} islands on C_{70} after annealing at 423 K for one hour. The dark bands persist. Individual "bright spots", identified as C_{70} molecules, appear within the C_{60} islands. (b) After one hour annealing to 473 K, more bright spots appears in the C_{60} layer. (55 nm × 45 nm, -2.5 V, 100 pA) (c) Annealed to 523 K for one hour, there is a huge increase in the number of C_{70} molecules in the second layer. The distribution of C_{70} molecules is very non-uniform. (90 nm × 90 nm, -2.5 V, 100 pA) (d) Height profile along line J-K in (a). The C_{70} molecule is seen by its characteristic height, being 0.10 nm taller than C_{60} in the same layer.

Based on the above analysis, we can draw a few conclusions on C_{60}-on-C_{70}. i) The "close-packed" single C_{70} layer on Au(111) consists of molecules in a state of random rotation with nearest a neighbor distance of ~ 1.07 nm. ii) When C_{60} molecules are deposited onto the C_{70} layer at RT, they can squeeze into the C_{70} layer, forcing the C_{70} molecules to change their orientation. iii) A nearly strain-free interface can be formed between a close packed C_{60} layer and a close packed C_{70} layer. This is facilitated by C_{70} taking an upright orientation to lattice match with C_{60}. iv) Molecular transport across the C_{60}-C_{70} interface takes place at elevated temperatures leading to mixing of C_{60} and C_{70} in each layer.

3.2.2 0.65ML C_{70} deposited on top of 1.0 ML C_{70} (C_{70}-on-C_{70})

In the previous section, we discussed orientational ordering of C_{70} in the first layer upon the addition of an overlayer of C_{60}. In this section, we examine the growth of the second layer C_{70} on top of a first layer C_{70}. Figure 8(a) shows an STM image acquired from the Au(111) sample after 0.65 ML of C_{70} is deposited at RT onto a preformed full C_{70} monolayer. The first C_{70} monolayer here has the R30^{o} structure. The first, second and third molecular layers are highlighted by the numbers 1, 2, and 3 respectively. Third layer C_{70} islands appear well before the completion of the second layer. The height profile along the line P-Q in Fig. 8(b) shows that the second layer is ~0.75 nm above the first layer and the third layer is ~0.75 nm above the second layer. These numbers are in good agreement with the height of the second layer C_{70} on HOPG. Fig. 8(c) is a high-resolution image. The second and third layers of C_{70} appear rather uniform with very few dim molecules.

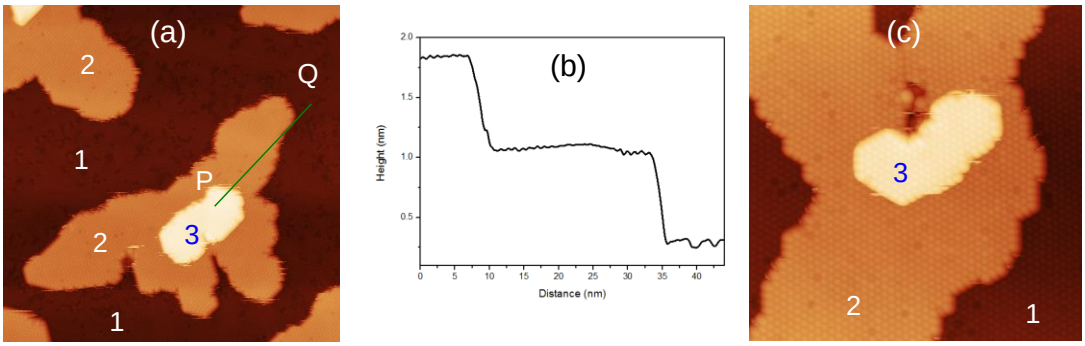

Figure 8. (a) 0.65 ML C_{70} deposited onto one compact monolayer C_{70} layers on Au (111). The first layer, 1, is a compact monolayer of C_{70}. The second, 2, and third, 3, layers are formed upon the deposition of the extra 0.65 ML of C_{70}. (100 nm × 100 nm, -2.5 V, 100 pA). (b) Height profile along line P-Q in (a). The heights of the second and the third layer C_{70} are similar and are approximately 0.75 nm. (c) High-resolution image. The second and third layers of C_{70} appear rather smooth with very few dim molecules.

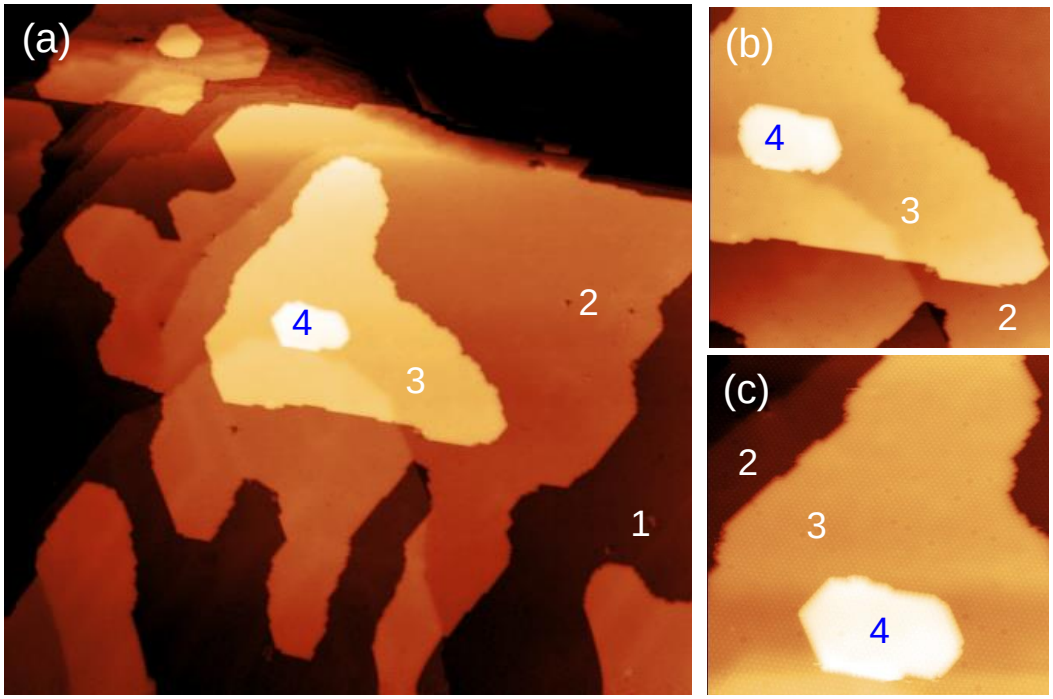

Figure 9. (a) STM image, (270 nm × 270 nm, -2.5 V, 100 pA), showing C_{70} on Au (111) annealed for one hour at 423 K. There is a noticeable increase in the average size of the molecular islands for both the second and the third layers. In some places, small-sized 4^{th} layer islands have appeared. Magnified views are shown in (b) (100 nm × 100 nm, -2.5 V, 100 pA) and (c) (65 nm × 65 nm, -2.5 V, 100 pA).

Annealing at 423 K leads to ripening of the molecular islands. The average size of the molecular islands increases for both the second and third layers. The edges of the islands become more smooth and appear faceted. The coverage of the third layer has increased from 0.04ML to 0.12ML, suggesting that a significant number of molecules have moved from the second layer upwards. We even observe the formation of molecular islands in the fourth layer, Fig. 9. It is more than likely that molecular exchange has taken place between the layers, although such a process is difficult to identify because there is only one type of molecule in all layers. The formation of the fourth layer island is a strong piece of evidence that molecules from lower layers have jumped up into the higher layers during annealing. This represents a typical coarsening effect. After annealing to 473 K and above, the third and the forth layers have disappeared due to thermal desorption, Figure 10.

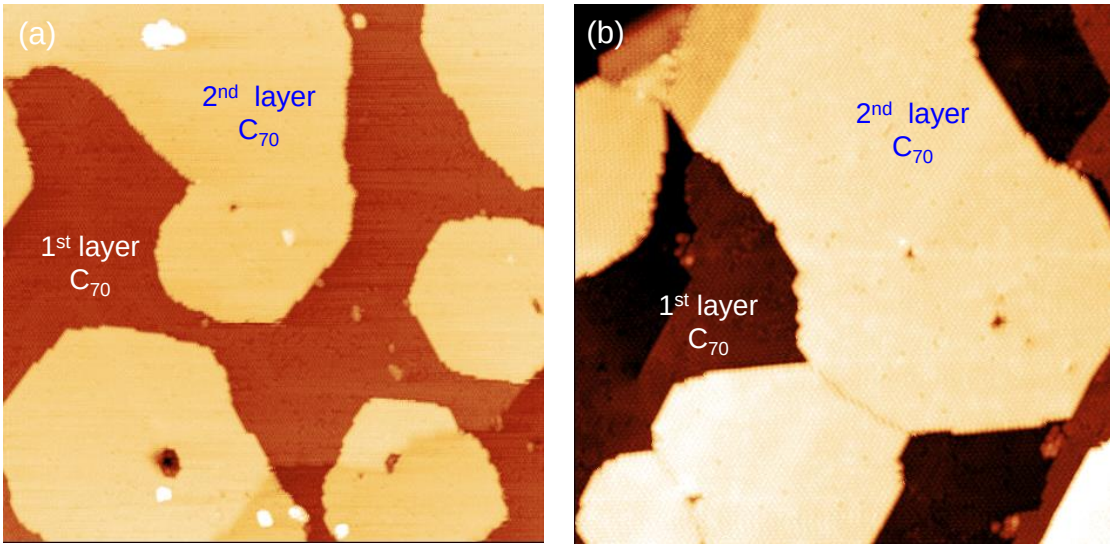

Figure 10. (a) STM image, (165 nm × 165 nm, -2.5 V, 100 pA), showing the morphology of the C_{70} layers after annealing to 473 K for one hour. (b) (120 nm × 120 nm, -2.5 V, 100 pA), showing the morphology of the C_{70} layers after annealing to 523 K for one hour.

3.2.3 0.65ML C_{70} deposited on top of 1.0 ML C_{60} (C_{70}-on-C_{60})

Data presented in section 3.2.1 demonstrate that the first layer C_{70} preformed on Au(111) can accommodate extra C_{60} molecules by altering the molecular orientation. In this section, we investigate how a preformed C_{60} layer on Au(111) responds to the addition of C_{70} molecules. We first deposit 1.2 ML C_{60} onto bare Au(111). We then anneal the sample to 673 K for one hour to remove molecules in the second layer. This produces a single layer of C_{60} covering nearly 100% of the gold substrate. The C_{60} layer consists of mostly R30° and R0° phases. The image in Figure 11(a) shows C_{70} islands formed on an R30° C_{60} layer. "1, C_{70}" and "2, C_{70}" mark the first and second layer C_{70}, respectively. The real first layer, however, is the C_{60} layer in direct contact with Au(111). A height profile along line R-S in (a) is shown in Fig. 11(b). From the height profile, we find that the first C_{70} layer (1,C_{70}) is ~ 0.88 nm above the C_{60} layer. Thus, the C_{70} layer on C_{60} appears taller than the C_{70} layer on C_{70} (Fig. 8(b). We interpret this height difference being due to different molecular orientations. For C_{70} on C_{70}, molecules in both C_{70} layers are in their free rotating state. Here, for C_{70} on C_{60}, the C_{70} layer is lattice-matched with the C_{60} layer below and the lattice-matching is achieved by C_{70} molecules sitting in the three-fold hollow site of the C_{60} layer with their long axis perpendicular to the C_{70}/C_{60} interface. Magnified views such as the one shown in Fig. 11(c) can be used to identify the adsorption site of C_{70} on C_{60}. We find that the C_{70} molecules sit exactly on the three-fold hollow site of the C_{60} layer. C_{70} molecules in the (2,C_{70}) layer sit on the three-fold hollow sites provided by the (1,C_{70}) layer. Hence, they also take the upright orientation.

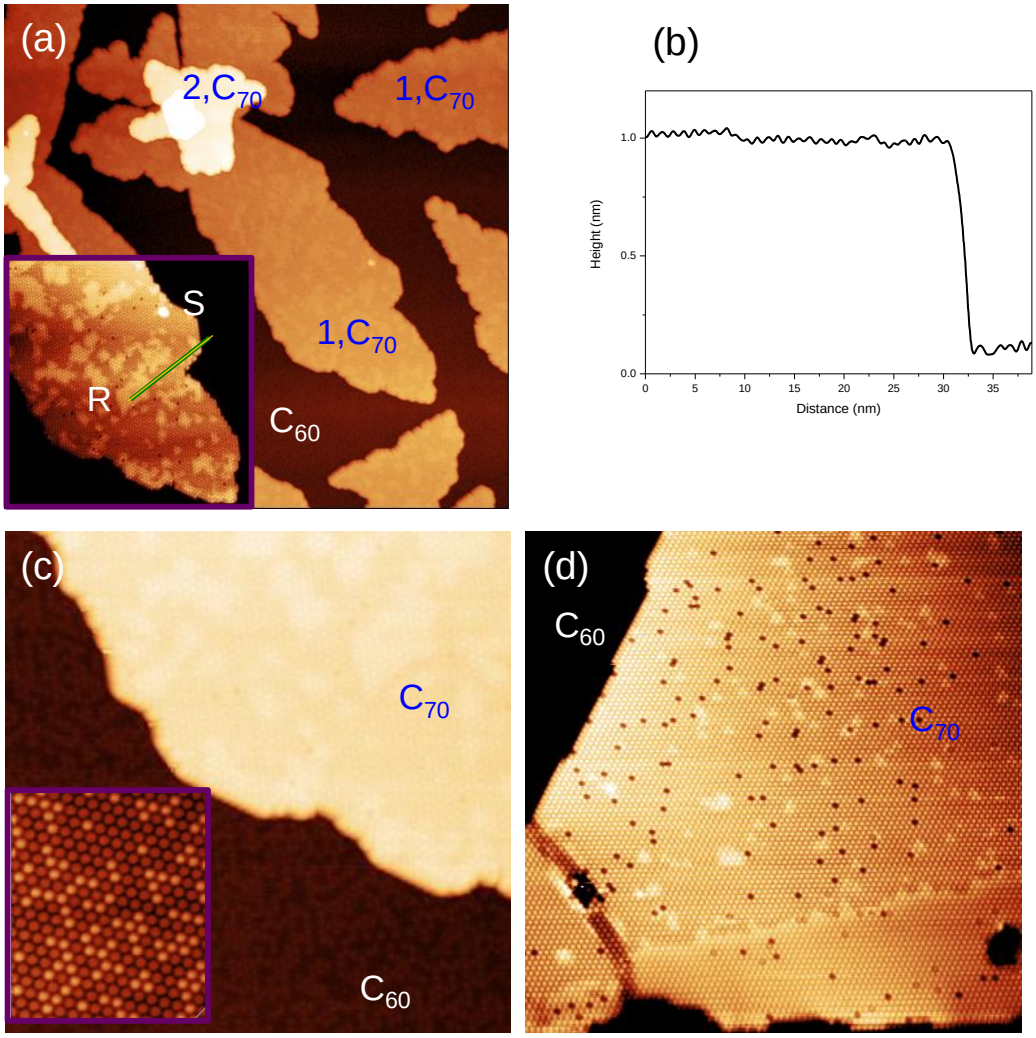

Figure 11. (a) STM images (80 nm × 80 nm, -2.5 V, 100 pA) showing C_{70} islands formed on top of a compact C_{60} layer following the deposition of 0.65 ML C_{70} at RT. Inset highlights the irregular bright patches. (b) Height profile along line R-S in (a) showing that the C_{70} island is 0.88 nm above the initial C_{60} layer. (c) Magnified view (65 nm × 65 nm, -2.5 V, 100 pA) with inset showing the typical "bright" and "dim" C_{60} molecules. (d) Image (80 nm × 80 nm, -2.5 V, 100 pA) acquired after thermal annealing to 523 K for one hour.

The inset in Fig. 11(c) shows that the C_{60} molecules in the R30° phase can be divided into the "bright' and the "dim" molecules [37,40,42]. There is no change to the morphology of the C_{60} layer after adding C_{70}. There is no evidence that C_{70} molecules have been incorporated into the C_{60} layer. This is not surprising considering that the C_{60} layer is a close-packed compact layer, so a lot of energy would be required to insert C_{70} molecules into the C_{60} layer. The (1,C_{70}) layer shows some irregular bright patches, Fig. 11(a) inset. This is a direct consequence of the molecular bonding that takes place between the C_{60} and the C_{70} layers. In a previous study[49], we found similar patchy features when C_{60} islands are formed on top of a C_{60} layer. The bright patches were explained being due to the organisation of Au atoms. The presence of the "bright"

and “dim” C_{60} molecules suggests non-uniform bonding between C_{60} and Au(111), for example, the possibility of surface atomic vacancies. When C_{70} or C_{60} is added on top of the first layer C_{60}, the bonding between the two molecular layers weakens the interaction between Au(111) and the molecules in the first layer allowing atomic vacancy to move.

When the sample is heated to higher temperatures, dim spots start to appear within the C_{70} layer as shown in Fig. 11(d). This could be a sign of molecular exchange between the C_{70} layer and the C_{60} layer underneath. If so, the extent of molecular exchange is rather limited, indicating that the first layer C_{60} is rather stable. There are also changes to the shape of the bright patches that become more regular triangles. As already stated, these bright patches originate from the atomic packing on the Au(111) surface, although the exact nature is not quite clear yet.

4. Conclusions

A few conclusions are drawn from our experimental findings.
(1) For the first molecular layer consisting of both C_{60} and C_{70} on Au(111), the molecules tend to form separated C_{60}-rich and C_{70} rich domains. Edge-dislocations are found at domain boundaries due to lattice mismatch. The C_{60}-rich domain contains trapped C_{70} molecules. The trapped C_{70} molecules take an upright configuration with their long molecular axis perpendicular to the substrate.

(2) The molecules within the first C_{70} layer are in a free-rotating state at RT. C_{70} molecules can change their orientation from free-rotating to an upright configuration when C_{60} molecules are added. Post-deposited C_{60} molecules can squeeze into the C_{70} layer. By incorporating up to ~ 14% of C_{60} molecules into the first layer of C_{70}, the combined C_{60}/C_{70} layer has a higher density with a nearest molecular distance almost equal to that in a pure C_{60} layer.

(3) C_{70} molecules form a lattice-matched second layer on top of the first layer of C_{60}. The lattice-matched growth forces the C_{70} molecules in the second layer to take an up right orientation. The C_{70} molecules sitting above the C_{60} layer are orientationally frozen at RT.

(4) Substantial interlayer molecular transport is observed at elevated temperatures. Since C_{60} is bound to Au(111) more strongly than C_{70}, there is a tendency for C_{70} molecules to move up creating space for C_{60} to drop down into the first layer.

Acknowledgements

We thank the Chinese Scholarship Council for providing a studentship to Lu'an Guo.

References

[1] Talapin, D. V.; Murray, C. B. PbSe nanocrystal solids for n- and p-channel thin film field-effect transistors. *Science.* **2005**, *310*, 86-89.

[2] Weissman, J. M.; Sunkara, H. B.; Tse, A. S.; Asher, S. A. Thermally switchable periodicities and diffraction from mesoscopically ordered materials. *Science.* **1996**, *274*, 959-963.

[3] Dong, A.; Chen, J.; Vora, P. M.; Kikkawa, J. M.; Murray, C. B. Binary nanocrystal superlattice membranes self-assembled at the liquid–air interface. *Nature.* **2010**, *466*, 474-477.

[4] Kim, S.; Ishii, S.; Yagi, R.; Kuwahara, Y.; Ogata, T.; Kurihara, S. Photo-induced orientation behaviors of azobenzene liquid crystal copolymers for photonic crystals. *RSC Adv.* **2017**, *7*, 51978-51985.

[5] Ding, S.; Liu, Y.; Li, Y.; Liu, Z.; Sohn, S.; Walker, F. J.; Schroers, J. Combinatorial development of bulk metallic glasses. *Nat. Mater.* **2014**, *13*, 494-500.

[6] Furukawa, H.; Cordova, K. E.; O'Keeffe, M.; Yaghi, O. M. The chemistry and applications of metal-organic frameworks. *Science.* **2013**, *341*, 1230444.

[7] Huang, Y. B.; Liang, J.; Wang, X. S.; Cao, R. Multifunctional metal–organic framework catalysts: synergistic catalysis and tandem reactions. *Chem. Soc. Rev.* **2017**, *46*, 126-157.

[8] Demirörs, A. F.; Pillai, P. P.; Kowalczyk, B.; Grzybowski, B. A. Colloidal assembly directed by virtual magnetic moulds. *Nature.* **2013**, *503*, 99-103.

[9] Redl, F. X.; Cho, K. S.; Murray, C. B.; O'Brien, S. Three-dimensional binary superlattices of magnetic nanocrystals and semiconductor quantum dots. *Nature.* **2003**, *423*, 968-971.

[10] Kiely, C. J.; Fink, J.; Brust, M.; Bethell, D.; Schiffrin, D. J. Spontaneous ordering of bimodal ensembles of nanoscopic gold clusters. *Nature.* **1998**, *396*, 444-446.

[11] Shevchenko, E. V.; Talapin, D. V.; Rogach, A. L.; Kornowski, A.; Haase, M.; Weller, H. Colloidal synthesis and self-assembly of $CoPt_3$ nanocrystals. *J. Am. Chem. Soc.* **2002**, *124*, 11480-11485.

[12] Russell, J. L.; Noel, G. H.; Warren, J. M.; Tran, N. L.; Mallouk, T. E. Binary colloidal crystal films grown by vertical evaporation of silica nanoparticle suspensions. *Langmuir.* **2017**, *33*, 10366-10373.

[13] Shevchenko, E. V.; Talapin, D. V.; Kotov, N. A.; O'Brien, S.; Murray, C. B. Structural diversity in binary nanoparticle superlattices. *Nature.* **2006**, *439*, 55-59.

[14] O'Toole, P. I.; Hudson, T. S. New high-density packings of similarly sized binary spheres. *J. Phys. Chem. C.* **2011**, *115*, 19037-19040.

[15] Kalsin, A. M.; Fialkowski, M.; Paszewski, M.; Smoukov, S. K.; Bishop, K. J. M.; Grzybowski, B. A. Electrostatic self-assembly of binary nanoparticle crystals with a diamond-like lattice. *Science.* **2006**, *312*, 420-424.

[16] Shevchenko, E. V.; Kortright, J.; Talapin, D. V.; Aloni, S.; Alivisatos, A. P. Quasi-ternary nanoparticle superlattices through nanoparticle design. *Adv. Mater.* **2007**, *19*, 4183-4188.

[17] Paik, T.; Diroll, B. T.; Kagan, C. R.; Murray, C. B. Binary and ternary superlattices self-assembled from colloidal nanodisks and nanorods. *J. Am. Chem. Soc.* **2015**, *137*, 6662-6669.

[18] Dong, A.; Ye, X.; Chen, J.; Murray, C. B. Two-dimensional binary and ternary nanocrystal superlattices: the case of monolayers and bilayers. *Nano Lett.* **2011**, *11*, 1804-1809.

[19] Denkov, N.; Velev, O.; Kralchevski, P.; Ivanov, I.; Yoshimura, H.; Nagayama, K. Mechanism of formation of two-dimensional crystals from latex particles on substrates. *Langmuir*. **1992**, *8*, 3183-3190.

[20] Singh, G.; Pillai, S.; Arpanaei, A.; Kingshott, P. Layer-by-Layer growth of multicomponent colloidal crystals over large areas. *Adv. Funct. Mater.* **2011**, *21*, 2556-2563.

[21] Lvov, Y.; Ariga, K.; Ichinose, I.; Kunitake, T. Assembly of multicomponent protein films by means of electrostatic layer-by-layer adsorption. *J. Am. Chem. Soc.* **1995**, *117*, 6117-6123.

[22] Kovtyukhova, N. I.; Ollivier, P. J.; Martin, B. R.; Mallouk, T. E.; Chizhik, S. A.; Buzaneva, E. V.; Gorchinskiy, A. D. Layer-by-layer assembly of ultrathin composite films from micro-sized graphite oxide sheets and polycations. *Chem. Mater.* **1999**, *11*, 771-778.

[23] Richardson, J. J.; Cui, J.; Björnmalm, M.; Braunger, J. A.; Ejima, H.; Caruso, F. Innovation in layer-by-layer assembly. *Chem. Rev.* **2016**, 116, 14828-14867.

[24] Pothorszky, S.; Zambo, D.; Deak, T.; Deak, A. Assembly patchy nanorods with spheres: limitations imposed by colloidal interactions. *Nanoscale.* **2016**, *8*, 3523-3529.

[25] Adams, M.; Fraden, M. Phase behavior of mixtures of rods (tobacco mosaic virus) and spheres (polyethylene oxide, bovine serum albumin). *Biophys. J.* **1998**, 74, 669-677.

[26] Ye, X.; Millan, J. A.; Engel, M.; Chen, J.; Diroll, B. T.; Glotzer, S. C.; Murray, C. B. Shape alloys of nanorods and nanospheres from self-assembly. *Nano Lett*. **2013**, *13*, 4980-4988.

[27] Yannoni, C. S.; Bernier, P. P.; Bethune, D. S.; Meijer, G.; Salem, J. R. NMR determination of the bond lengths in C_{60}. *J. Am. Chem. Soc.* **1991**, *113*, 3190-3192.

[28] Heiney, P. A.; Fischer, J. E.; McGhie, A. R.; Romanow, W. J.; Denenstein, A. M.; McCauley, J.; John, P.; Smith, A. B.; Cox, D. E. Orientational ordering transition in solid C_{60}. *Phys. Rev. Lett.* **1991**, *66*, 2911.

[29] Dresselhaus, M. S.; Dresselhaus, G.; Eklund, P. C. *Science of fullerenes and carbon nanotubes: their properties and applications*. *Elsevier*. **1996**.

[30] Hedberg, K.; Hedberg, L.; Bethune, D. S.; Brown, C. A.; Dorn, H. C.; Johnson, R. D.; De Vries, M. Bond lengths in free molecules of buckminsterfullerene, C_{60}, from gas-phase electron diffraction. *Science.* **1991**, *254*, 410-412.

[31] McKenzie, D. R.; Davis, C. A.; Cockayne, D. J. H.; Muller, D. A.; Vassallo, A. M. The structure of the C_{70} molecule. *Nature.* **1992**, *355*, 622.

[32] Altman, E. I.; Colton, R. J. The interaction of C_{60} with noble metal surfaces. *Surf. Sci.* **1993**, *295*, 13-33.

[33] Schull, G.; Berndt, R. Orientationally ordered (7× 7) superstructure of C_{60} on Au (111). *Phys. Rev. Lett.* **2007**, *99*, 226105.

[34] Gardener, J. A.; Briggs, G. A. D.; Castell, M. R. Scanning tunneling microscopy studies of C_{60} monolayers on Au (111). *Phys. Rev. B*. **2009**, *80*, 235434.

[35] Guo, S.; Fogarty, D. P.; Nagel, P. M.; Kandel, S. A. Thermal diffusion of C_{60} molecules and clusters on Au (111). *J. Phys. Chem. B.* **2004**, *108*, 14074-14081.

[36] Rogero, C.; Pascual, J. I.; Gomez-Herrero, J.; Baro, A. M. Resolution of site-specific bonding properties of C_{60} adsorbed on Au (111). *J. Chem. Phys.* **2002**, *116*, 832-836.

[37] Zhang, X.; Yin, F.; Palmer, R. E.; Guo, Q. The C_{60}/Au (111) interface at room temperature: A scanning tunnelling microscopy study. *Surf. Sci*. **2008**, *602*, 885-892.
[38] Tang, L.; Zhang, X.; Guo, Q.; Wu, Y. N.; Wang, L. L.; Cheng, H. P. Two bonding configurations for individually adsorbed C_{60} molecules on Au (111). *Phys. Rev. B.* **2010**, *82*, 125414.
[39] Tang, L.; Xie, Y. C.; Guo, Q. Complex orientational ordering of C_{60} molecules on Au (111). *J. Chem. Phys.* **2011**, *135*, 114702.
[40] Xie, Y. C.; Tang, L.; Guo, Q. Cooperative assembly of magic number C_{60}-Au complexes. *Phys. Rev. Lett.* **2013**, *111*, 186101.
[41] Kaya, D.; Bao, D.; Palmer, R. E.; Du, S.; Guo, Q. Tip-triggered thermal cascade manipulation of magic number gold–fullerene clusters in the scanning tunnelling microscope. *Nano Lett.* **2017**, *17*, 6171-6176.
[42] Xie, Y. C.; Rokni Fard, M.; Kaya, D.; Bao, D.; Palmer, R. E.; Du, S.; Guo, Q. Site-specific assembly of fullerene nanorings guided by two-dimensional gold clusters. *J. Phys. Chem. C.* **2016**, *120*, 10975-10981.
[43] Barth, J. V.; Brune, H.; Ertl, G.; Behm, R. Scanning tunneling microscopy observations on the reconstructed Au (111) surface: Atomic structure, long-range superstructure, rotational domains, and surface defects. *Phys. Rev. B.* **1990**, *42*, 9307.
[44] Guo, Q.; Yin, F.; Palmer, R. E. Beyond the herringbone reconstruction: magic gold fingers. *Small.* **2005**, *1*, 76-79**.**
[45] Vaughan, G. B.; Heiney, P. A.; Cox, D. E.; Fischer, J. E.; McGhie, A. R.; Smith, A. L.; Strongin, R. M.; Cichy, M. A.; Smith III, A. B. Structural phase transitions and orientational ordering in C_{70}. *Chem. Phys*. **1993**, *178*, 599-613.
[46] Guo, Lu'an; Wang, Y. T.; Kaya, D.; Palmer, R. E.; Chen, G-D.; Guo, Q. Orientational epitaxy of Van der Waals molecular heterostructures. *Nano Lett*. 2018. DOI: 10.1021/acs.nanolett.8b02238.
[47] Barth, J. V.; Schuster, R.; Behm, R. J.; Ertl, G. The system K/Au (111): adsorption and surface restructuring. *Surf. Sci.* **1996**, *348*, 280-286.
[48] Rossel, F.; Brodard, P.; Patthey, F.; Richardson,N. V.; Schneider, W-D. Modified herringbone reconstruction on Au (111) induced by self-assembled Azure A islands. *Surf. Sci*. **2008**, *602*, L115-L117.
[49] Tang, L.; Guo, Q. Orientational ordering of the second layer of C_{60} molecules on Au (111). *Phys. Chem. Chem. Phys.* **2012**, *14*, 3323-3328.

TOC graphic